

www.acsami.org Research Article

High-Purity and Saturated Deep-Blue Luminescence from *trans*-NHC Platinum(II) Butadiyne Complexes: Properties and Organic Light Emitting Diode Application

Ru He, Zhengtao Xu, Silvano Valandro, Hadi D. Arman, Jiangeng Xue, and Kirk S. Schanze*



Cite This: ACS Appl. Mater. Interfaces 2021, 13, 5327-5337



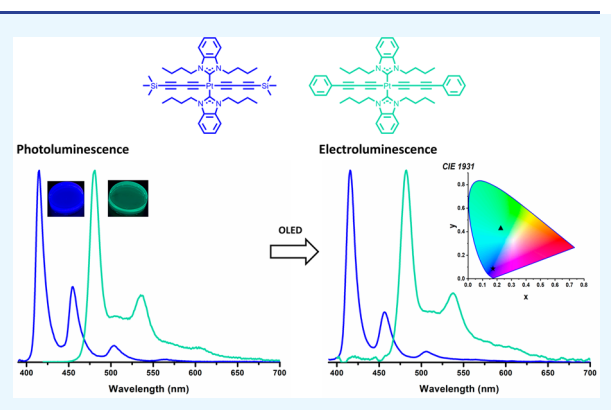
ACCESS

III Metrics & More

Article Recommendations

s Supporting Information

ABSTRACT: Two new platinum(II) compounds with *trans*-(NHC)₂Pt(C≡C−C≡C−R)₂ (where NHC = N-heterocyclic carbene and R = phenyl or trimethylsilyl) architecture exhibit sharp blue-green or saturated deep-blue phosphorescence with high color purity. The photoluminescence of both compounds is dominated by an intense 0−0 band with distinct but weaker vibronic progressions in both tetrahydrofuran (THF) and poly(methyl methacrylate) (PMMA) matrix. The full width at half-maximum (fwhm) of the photoluminescence of *trans*-(NHC)₂Pt(C≡C−C≡C-trimethylsilyl)₂ are 10 nm at room temperature and 4 nm at 77 K, while the *trans*-(NHC)₂Pt(C≡C−C≡C-phenyl)₂ shows a fwhm of 14 nm at room temperature and 8 nm at 77 K. The Commission International de L'Eclairage (CIE) coordinates of *trans*-(NHC)₂Pt(C≡C−C≡C-phenyl)₂ are (0.222, 0.429) in PMMA, and *trans*-(NHC)₂Pt(C≡C−C≡C-phenyl)₂ are (0.222, 0.429) in PMMA, and *trans*-(NHC)₂Pt(C≡C−C≡C-phenyl)₂ are (0.222, 0.429) in PMMA, and *trans*-(NHC)₂Pt(C≡C−C≡C-phenyl)₂ are



C \equiv C-trimethylsilyl)₂ has a deep-blue CIE of (0.163, 0.077) in PMMA. When doped into PMMA, the phosphorescence quantum yield of the complex with trimethylsilyl-butadiyne ligand increases dramatically to 57% from 0.25% in THF, while the complex with phenyl-butadiyne ligand has similar quantum yields in PMMA (32%) and THF (37%). Organic light-emitting diodes (OLEDs) employing these two complexes as the emitters were successfully fabricated with electroluminescence that closely matches the corresponding photoluminescence. The OLEDs based on trans-(NHC)₂Pt(C \equiv C-C \equiv C-trimethylsilyl)₂ display highly pure deep-blue electroluminescence (fwhm = 12 nm) with CIE coordinates of (0.172, 0.086), approaching the most stringent National Television System Committee (NTSC) coordinates for "pure" blue of (0.14, 0.08).

KEYWORDS: platinum(II) complex, N-heterocyclic carbene, phosphorescence, photoluminescence, electroluminescence, OLED

■ INTRODUCTION

Organic light-emitting diodes (OLEDs) featuring an emissive layer of organic electroluminescent materials have been successfully applied to create digital displays for televisions and portable devices. 1-3 In contrast to well-defined lightemitting diodes (LEDs) based on semiconductors like gallium nitride (GaN), OLEDs are thinner and more flexible with a lower cost.⁴⁻⁶ Recently, the efficiencies of OLEDs have been dramatically improved by employing phosphorescent metal complexes that can harvest both singlet and triplet excitons for light emission, and the theoretical internal quantum efficiency can approach 100%. The ongoing development of phosphorescent OLEDs (PHOLEDs) has already achieved the breakthrough in red and green electrophosphorescent devices. 9-13 However, as a type of OLED, PHOLEDs generally display broad emission bands (fwhm >40 nm) due to structural relaxation and vibronic coupling; thus color filters or optical microcavities are required to improve the color purity, leading to significant power loss. 14-16 Achieving higher

emission color purity remains as one of the pressing challenges for future PHOLEDs development.

As one of the three primary colors, blue emission is very important in full-color displays. Unlike the rapid progress in red and green PHOLEDs, efficient, pure deep blue emission of PHOLEDs remains a challenge. Despite the fact that intense efforts have been made by many research groups in recent years, the significant drawbacks of demonstrated deep blue PHOLEDs are their relatively dissatisfactory Commission International de L'Eclairage (CIE) coordinates, poor color purity, and low efficiency. ¹⁷ The commonly reported deep blue PHOLEDs display broad emission bands (fwhm >40 nm) and

Received: November 28, 2020 Accepted: January 11, 2021 Published: January 21, 2021





the corresponding CIE coordinates fall near (0.15, 0.15). 14,16,18,19 The pronounced vibronic progression of the phosphorescence of metal complexes makes it difficult for CIE $_y$ value to be lower than 0.1. To achieve the National Television System Committee (NTSC) coordinates for "pure" blue of (0.14, 0.08) with narrow spectral bandwidth, a substantial amount of the emission outside the deep-blue region (>500 nm) must be suppressed or the triplet energy must be increased. 18,19

Many efforts have been made to tackle these broad challenges, and octahedral cyclometalated iridium(III) complexes attract most of the attention. By modification of the cyclometalating ligands in homoleptic iridium(III) complexes or the ancillary ligands in heteroleptic complexes, the emission color can be tuned from orange-red to blue. High-field-strength N-heterocyclic carbenes (NHCs) are widely used as ligands in blue-emitting iridium(III) based complexes. The strong σ -donating nature of NHCs destabilizes the metal-centered ligand-field states, leading to a profound improvement in the emission performances of PHOLEDs. The NHC iridium(III) complex, fac-Ir(pmp)₃, based PHOLED reported by Forrest et al. exhibits CIE coordinates of (0.16, 0.09), close to the NTSC requirement for blue color.

Although remarkable progress has been achieved on iridium(III) complexes based PHOLEDs, overemphasis on one group of materials can potentially restrict the scope of the development of OLEDs.²⁷ Thus, many studies have also been carried out to apply different chromophores such as square planar platinum(II) complexes for OLED applications, which diversify the efforts for electroluminescent materials development.27,28 Our group has previously reported a trans-NHC platinum(II) acetylide complex featuring phenyl-acetylide ligands (NPtPE1) with CIE coordinates of (0.14, 0.12) in PMMA matrix and (0.2, 0.2) in a device.²⁹ In comparison to trans-Pt(PR₃)₂(CC-Ar)₂ complexes, the incorporation of NHC ligands into trans-Pt(NHC)₂(CC-Ar)₂ architecture enables efficient phosphorescence from relatively high energy ${}^3\pi$, π * states that are based on the CC-Ar ligands.²⁹ However, relatively poor emission color purity and CIE coordinates in devices still hinder the application of trans-NHC platinum(II) acetylide complexes in OLEDs.

In the present work, we address the two main challenges, color purity and pure deep blue emission. This has been done via careful molecular structure design to introduce the two new trans-NHC platinum(II) compounds (BiPtDyTMS and BiPtDyP, Chart 1) featuring butadiyne functionalities with improved luminescence color purity. From a fundamental perspective, oligo-yne is one of the simplest linear extended π -conjugated systems. By increasing the number of triple bonds, we can slightly tune the conjugation of the acetylide ligands, thereby modifying the phosphorescence that originates from

Chart 1. Structures of (a) BiPtDyTMS and (b) BiPtDyP

the butadiyne ligand-centered $^3\pi$, π^* states of *trans*-NHC platinum(II) complexes. $^{29-31}$ With phenyl-butadiyne ligands instead of phenyl-acetylene ligands, BiPtDyP shows a bluegreen photoluminescence with a surprisingly sharper emission shape than the previously reported trans-NHC platinum(II) acetylides complex BiPtP.³² This is due to the well-defined C≡C vibronic modes that dominate the phosphorescence emission spectrum. BiPtDyP based PHOLEDs exhibit CIE coordinates of (0.225, 0.427) with a sharp blue-green electroluminescence shape, which is identical to the photoluminescence. By incorporating the simplest oligo-yne ligand, trimethylsilyl-butadiyne, into the trans-NHC platinum(II) architecture, the as-obtained BiPtDvTMS displays a surprisingly high-purity deep-blue luminescence both in solution and in solid-state with a narrow spectral bandwidth (fwhm = 10 nm) even at room temperature. In previous related work, Che and co-workers reported that the digold(I) complex (Cy₃P)- $Au-C \equiv C-C \equiv C-Au(PCy_3)$ shows an emission maximum at 417 nm with a simple vibronic structure and sharp $v(C \equiv C)$ progressions in solution at ambient temperature; the emission bands are assigned to the bridging butadiyne ligand centered $^{3}\pi$, π^{*} excited states. 33 OLEDs that incorporate **BiPtDyTMS** as the phosphor exhibit CIE coordinates of (0.172, 0.086) and a narrow fwhm of 12 nm, which nearly meets the most stringent NTSC standards. Owing to the short conjugation length of trimethylsilyl-butadiyne ligand, the resulting high triplet energy and simple vibronic structure of BiPtDvTMS ensure the saturated deep-blue luminescence. This work provides some new concepts into the structural designs of phosphorescent materials to improve color purity and achieve pure deep-blue

■ RESULTS AND DISCUSSION

Synthesis and Characterization. Scheme 1 outlines the synthesis procedures of **BiPtDyTMS** and **BiPtDyP**, and details

Scheme 1. Synthesis of BiPtDyTMS and BiPtDyP.

are provided in the Supporting Information (Scheme S1). The precursor $BiPtCl_2$ was prepared through a one-pot/two-steps method involving the *in situ* formation of Ag(I)-NHC intermediate and subsequent transmetalation of the Ag(I)-NHC intermediate with K_2PtCl_4 . 32 BiPtDyTMS was readily prepared according to the reaction sequence shown in Scheme 1. Thus, the commercially available 1,4-bis(trimethylsilyl)-1,3-butadiyne was treated with MeLi-LiBr to remove one of the two trimethylsilyl (-TMS) groups. The as-formed lithium complex was quenched by triethylamine hydrochloride and

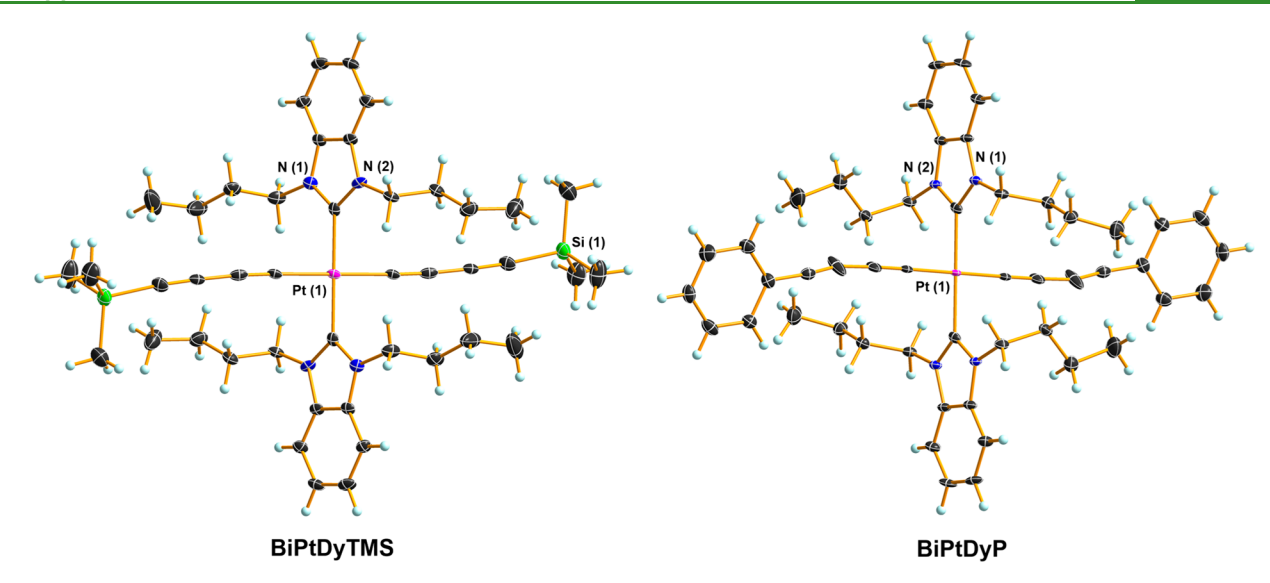


Figure 1. Crystal structures of BiPtDyTMS and BiPtDyP, with ellipsoids shown at the 50% probability level. Carbon atoms are shown in gray, and hydrogen atoms are shown in light turquoise; all are unlabeled.

Table 1. Selected Bond Lengths and Dihedral Angles from X-ray Crystal Structures

		bond leng	dihedral angle (deg)		
	Pt-C _{carbene}	Pt-C _{butadiyne}	PtC≡C	C≡CR ^a	N-C _{carbene} -N vs C _{carbene} -Pt-C _{butadiyne}
BiPtDyTMS	2.026(5)	1.988(6)	1.209(8)	1.213(8)	67.252
BiPtDyP	2.027(3)	1.989(3)	1.225(5)	С	86.114

^aR: -trimethylsilyl or -phenyl. ^bThe dihedral angle between the plane defined by N–C_{carbene}–N atoms on the carbene ligand and the plane defined by the Pt atom, a C_{carbene} atom, and a C_{butadiyne} atom (two C atoms directly connected to the Pt atom). ^cDue to the disorder of the phenyl ring.

subjected to Hagihara conditions in one-pot to give BiPtDyTMS. BiPtDyP was synthesized under similar Hagihara reaction conditions using BiPtCl₂ and 1-phenyl-1,3-butidiyne.

The structures and purity of final products were confirmed by ¹H NMR, ¹³C NMR, and high-resolution mass spectrometry (Supporting Information). The *trans* configuration of **BiPtDyTMS** and **BiPtDyP** was first confirmed by ¹H NMR. The two complexes showed a single multiplet between 4 and 5 ppm, which is assigned to the protons on the $-CH_2$ -connected to the NHC nitrogen atoms (NCH₂C₃H₇), while their *cis* isomers feature two multiplets. ³⁴ All the chemical shifts and integrations are matched well with the structures of the corresponding compounds.

The structures and geometries of BiPtDyTMS and BiPtDyP were further confirmed by single-crystal X-ray crystallography. Both structures were refined well and are shown in Figure 1. Selected bond lengths (Å) and dihedral angles (deg) are presented in Table 1, and detailed crystallographic data are reported in the Supporting Information. There is some disorder due to unrestricted torsion of the phenyl ring of BiPtDyP. X-ray crystallography confirms the trans configuration of the Pt(II)(NHC)2(butadiyne)2 center of both complexes, and the Pt atom resides in the inversion center of the molecule structure of each compound. Pt-C_{carbene} bond distances of BiPtDyTMS and BiPtDyP are 2.026(5) Å and 2.027(3) Å, respectively, and are very similar to the bond distances of previously reported Pt-NHC complexes from our group. 29,32 The Pt-C_{butadiyne} bond distances are 1.988(6) Å for **BiPtDyTMS** and 1.989(3) Å for **BiPtDyP**. The two triple bonds in the butadiyne ligands are slightly elongated and longer than triple bonds in acetylide ligands.³² The butadiyne moieties of both compounds are not completely linear, which is normal for sp carbon chains of polyynes and other platinum polyynediyl complexes. The dihedral angle between the NHC plane and the plane defined by $C_{carbene}-Pt-C_{butadiyne}$ of **BiPtDyTMS** is 67.252°, while the dihedral angle between the NHC plane and the plane of $C_{carbene}-Pt-C_{butadiyne}$ in **BiPtDyP** is 86.114°.

Photophysical Properties. UV—visible absorption spectra of **BiPtDyTMS** and **BiPtDyP** were recorded in THF solutions at room temperature and shown in Figure 2. The absorption

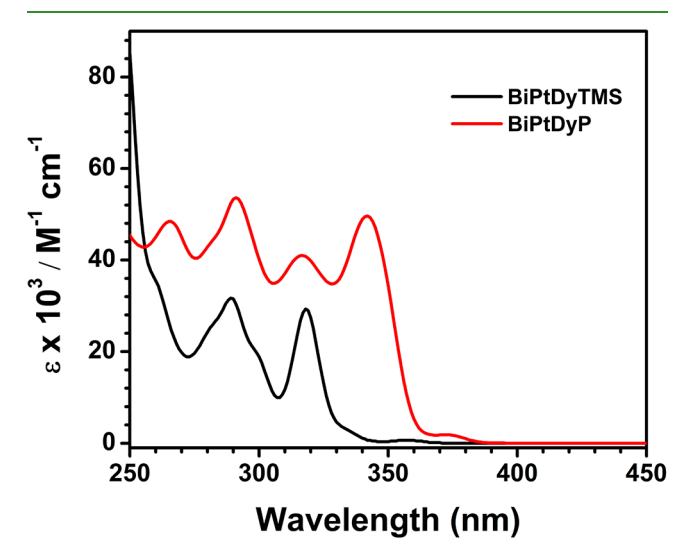


Figure 2. Overlaid UV—vis absorption of BiPtDyTMS and BiPtDyP in THF at room temperature.

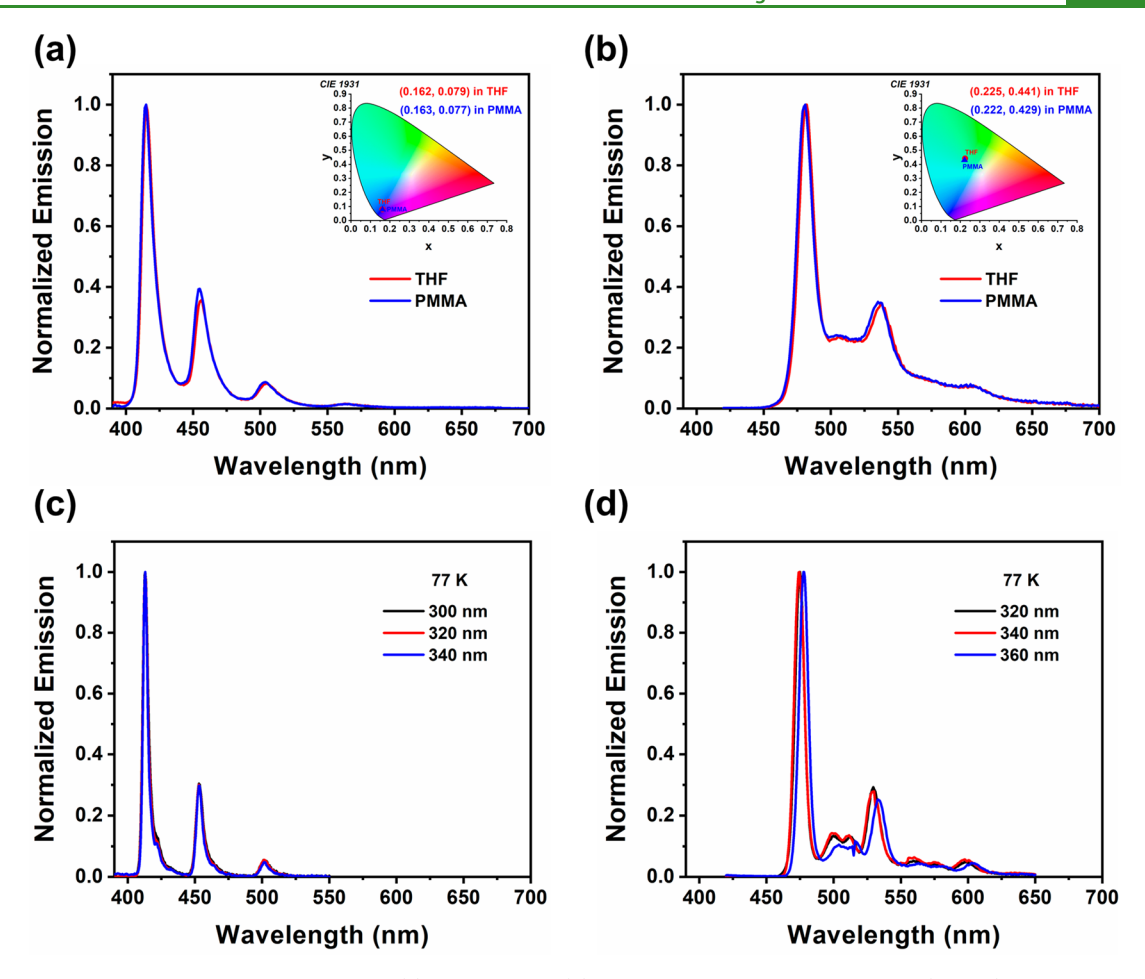


Figure 3. Photoluminescence spectra of **BiPtDyTMS** (a) and **BiPtDyP** (b) recorded in THF and PMMA films (2 wt %) at room temperature. The insets show the corresponding CIE coordinates. Photoluminescence spectra of **BiPtDyTMS** (c) and **BiPtDyP** (d) in 2-methyltetrahydrofuran at 77 K under different excitation wavelengths.

Table 2. Summary of Photoluminescence Data for BiPtDyTMS and BiPtDyP

	THF, RT				solid, RT ^a				
	λ, nm	$\Phi_{ ext{PL}}$	$ au^b$	(CIEx, CIEy)	λ, nm	$\Phi_{ ext{PL}}{}^c$	τ, μs ^b	(CIEx, CIEy)	Φ_{PL}^{c} (15 wt % in DPEPO)
BiPtDyTMS	415	0.0025	50.6 ns	(0.162, 0.079)	415	$0.57(2)$ $0.36(3)^d$	4.4	(0.163, 0.077)	0.38(7)
BiPtDyP	482	0.37	9.1 μs	(0.225, 0.441)	481	$0.32(1)$ $0.020(2)^d$	32.0	(0.222, 0.429)	0.29(3)

"Sample is 2 wt % complex in PMMA unless otherwise noted. ^bAll decays are biexponential except the phosphorescence lifetime of **BiPtDyTMS** in THF. The reported lifetime is a weighted average of the two lifetime components. For all lifetime measurements, $\lambda_{\rm exc} = 355$ nm. ^cAverage of three or four independent trials, with standard deviation of the last digit shown in parentheses. ^d15 wt % in PMMA.

spectrum of **BiPtDyTMS** is dominated by strong bands below 340 nm and a weak band at 340–370 nm, while **BiPtDyP** shows strong absorption bands between 250 and 365 and a weaker band at 365–385 nm. Distinct vibronic progressions are observed in the absorption spectra of both complexes which are associated with CC stretching modes. **BiPtDyP** shows an obvious red-shift in absorption and relatively larger molar extinction coefficient compared to **BiPtDyTMS**, apparently due to the increased conjugation due to the phenyl unit. The two long wavelength absorption bands seen for both complexes are due to transitions associated with two series of π -symmetry frontier orbitals arising from the butadiyne ligands and $d\pi(Pt)$ orbitals (see Supporting Information, Figure S21). ^{38,39} In particular, π_x (butadiyne) that is in plane with PtL₄ overlaps with $d_{xy}(Pt)$, and π_z (butadiyne) is perpendicular

to PtL₄ and overlaps with $d_{yz}(Pt)$. TDDFT calculations on related polyyne Pt complexes attribute the low energy absorption transitions to different configuration interactions of these two perpendicular basis frontier orbital sets.³⁹ In summary, the low energy absorption bands of **BiPtDyTMS** and **BiPtDyP** can be mainly attributed to butadiyne ligand centered $\pi \to \pi^*$ transitions with a minor contribution from metal-to-ligand charge transfer (MLCT).

Figure 3a and Figure 3b show the photoluminescence spectra of **BiPtDyTMS** and **BiPtDyP** in THF and in a poly(methyl methacrylate) (PMMA) glass at room temperature, whereas Table 2 summarizes the corresponding photoluminescence data. The photoluminescence of both complexes is assigned to phosphorescence from a $^3\pi$, π^* state based on the butadiyne ligands according to previous

studies. 29,32,40 The complex BiPtDyTMS displays identical photoluminescence in THF and when doped into PMMA at 2 wt % with the same λ_{max} = 415 nm (Figure 3a). The photoluminescence of BiPtDyTMS appears as a strong narrow 0-0 band (415 nm) accompanied by a vibronic progression (455, 504, and 564 nm) in a single frequency of \sim 2100 cm⁻¹, which can be assigned to the $v(C \equiv C)$ stretch.³³ The photoluminescence 0-0 band of BiPtDyTMS has a fullwidth at half-maximum (fwhm) of 10 nm (589 cm⁻¹). The sharpness and characteristic progression frequency (~2100 cm⁻¹) of the vibronic structure further confirm that the emissions of the two newly synthesized trans-Pt(II)-(NHC)₂(butadiyne)₂ complexes originate from the butadiyne ligand-localized ${}^3(\pi \to \pi^*)$ transitions. In THF media at room temperature, BiPtDyTMS shows a low phosphorescence quantum yield of 0.0025. By contrast, in PMMA glass, the phosphorescence quantum yield increases dramatically to 0.57 in the rigid environment. Replacing the trimethylsilyl group with phenyl (BiPtDyP) induces a red-shift of the emission maximum as shown in Figure 3b. The photoluminescence λ_{max} values of BiPtDyP in THF and PMMA (2 wt %) are 482 and 481 nm, respectively, with a small vibronic sideband at 537 nm and a narrow fwhm of 14 nm (596 cm⁻¹). The vibronic progression in the BiPtDyP spectrum is also dominated by the $v(C \equiv C)$ stretch (~2100 cm⁻¹); however, the bands are broadened due to the mixing of lower frequency vibrational modes involving the phenyl ring. The phosphorescence quantum yield of BiPtDyP in THF is reasonably high, 0.37. While in PMMA matrix, the quantum yield decreased slightly to 0.32. The emission quantum yields for both complexes were also measured at 15 wt % complex in PMMA and DPEPO (Figure S14 for structure), since this loading was used for the OLED testing (Table 2). As can be seen, the yields are similar in both solid hosts and are comparable to those for the 2 wt % PMMA films. One exception is BiPtDyP at 15 wt % in PMMA which shows a reduced quantum yield, presumably due to concentration quenching. Noteworthy is that BiPtDyP exhibits a high emission yield in the DPEPO host.

At room temperature, the photoluminescence decays in fluid solutions and PMMA films are biexponential except that of **BiPtDyTMS** in THF, which is monoexponential. All lifetimes are shown in Table 2 as weighted average lifetimes. The photoluminescence lifetime of **BiPtDyTMS** is 50.6 ns in THF and increases to 4.4 μ s in PMMA. **BiPtDyP** has a relatively longer lifetime in THF, 9.1 μ s, and the photoluminescence lifetime increases to 32.0 μ s when dispersed at 2 wt % in PMMA.

The radiative and nonradiative decay rates ($k_{\rm r}$ and $k_{\rm nr}$) respectively) for the complexes were computed from the phosphorescence quantum yields and lifetimes in solution and in the PMMA matrix (Table S3). For phenyl substituted complex BiPtDyP, both $k_{\rm r}$ and $k_{\rm nr}$ are comparable in magnitude and do not vary substantially in going from solution to the polymer matrix. This reflects the fact that the emission yield and lifetime for BiPtDyP do not change substantially in the different environments. However, in contrast, for the TMS substituted complex BiPtDyTMS, k_{nr} is \sim 400 times greater than k_r in THF, which indicates that for this complex in fluid solution excited state decay is dominated by a rapid nonradiative channel. By contrast, in the solid PMMA matrix, the values of $k_{\rm r}$ and $k_{\rm nr}$ are comparable, indicating that the nonradiative decay process is slowed substantially in the solid.

It is reported that trans-NHC platinum(II) acetylide complexes feature a nonemissive d-d excited state that lies just above the energy of the emitting ${}^{3}\pi_{1}\pi^{*}$ state. 32 The similar photophysical properties of BiPtDyP in solution and solidstate suggest that the nonemissive d-d excited state is not thermally accessible since the emitting state of BiPtDyP has a relatively low energy (2.6 eV). On the other hand, for **BiPtDyTMS** with a higher energy ${}^{3}\pi$, π * state (3.0 eV), the nonradiative metal-centered d-d state becomes thermally accessible. This leads to a low phosphorescence quantum yield that results from the rapid nonradiative path $(k_{\rm nr} \sim 2 \times 10^7)$ s⁻¹) which is likely dominated by the crossing to the d-d state.²⁶ According to our previous report on trans-NHC platinum(II) acetylide complexes, the access to the d-d state is accompanied by out-of-plane distortion of the square planar configuration of the complex.⁴¹ However, in the rigid PMMA matrix such distortion is prevented upon excitation of BiPtDyTMS, resulting in a dramatic enhancement of the phosphorescence quantum yield due to the dramatic reduction in $k_{\rm nr}$.

The photoluminescence spectra of both complexes can be considered to be sharp with high color purity, especially that of **BiPtDyTMS**. The CIE coordinates of **BiPtDyTMS** are (0.163, 0.077) in PMMA film, approaching the standard CIE coordinates of pure blue, (0.14, 0.08). Relatively high solid-state quantum yield, narrow emission band, and deep-blue photoluminescence color make **BiPtDyTMS** a potential emitter for deep-blue PHOLEDs. Due to the increased conjugation due to the phenylene ring, **BiPtDyP** displays a blue-green emission with CIE coordinates of (0.222, 0.429) in PMMA. Owing to the intense 0–0 band and relatively suppressed low energy vibronic bands, the emission color purity is also improved in comparison to previously reported *trans*-NHC platinum acetylide complexes.³²

Low temperature photoluminescence studies of BiPt-DyTMS and BiPtDyP were carried out in 2-methyltetrahydrofuran (2-MTHF) glass at 77 K, and spectra are shown in Figure 3c and Figure 3d. The emission spectra of BiPtDyTMS and BiPtDyP are much sharper with pronounced vibronic structures at 77 K when compared to their photoluminescence at room temperature (Figure 3a and Figure 3b), which is very characteristic for ligand centered ${}^3\pi,\pi^*$ excited state emission.²⁶ This further confirms that the photoluminescence of both complexes arises from ${}^{3}\pi_{1}\pi^{*}$ states that are based on butadiyne ligands. In Figure 3c, the emission spectra of BiPtDyTMS at 77 K still appear as a narrow 0-0 band with well-resolved narrow vibronic progressions at lower energy but are all blue-shifted when compared to its emission spectra in THF and PMMA at room temperature. The $\lambda_{\rm max}$ is shifted to 413 nm with a sharper vibronic structure than room temperature emission. The fwhm of BiPtDyTMS 0-0 band decreases to 4 nm at 77 K. By changing the excitation wavelength from 300 to 340 nm, no change in the emission spectrum is observed.

At 77 K, the emission spectrum of **BiPtDyP** is also sharper with a more distinct vibronic progression than observed in the room temperature spectrum (Figure 3d). Similar to **BiPtDyTMS**, the intense 0–0 band of **BiPtDyP** is blue-shifted and the fwhm decreases to 8 nm. Notably, by varying the excitation from 320 to 360 nm, two sets of emission onsets are observed with ~130 cm⁻¹ difference in frequency. This behavior is likely due to two nonequilibrating conformers of **BiPtDyP** that have different emission energy. Similar

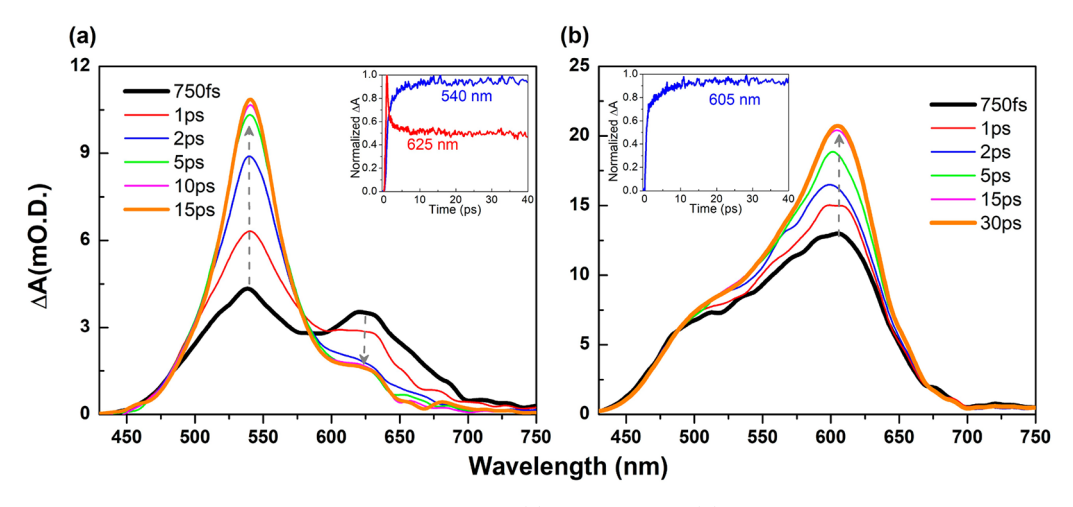


Figure 4. Femtosecond transient absorption spectra of BiPtDyTMS (a) and BiPtDyP (b) in THF with 330 nm and 100 μ J excitation. Inset: Kinetic traces of BiPtDyTMS and BiPtDyP.

observations were also reported for trans-Pt(PR₃)₂(CC-Ar)₂ and trans-Pt(NHC)₂(CC-Ar)₂ and were attributed to the nonequilibrating conformers in the glassy matrix that arise due to torsion of the aryl acetylide ligands.^{32,40} In the case of **BiPtDyP**, the active mode giving rise to the shift is torsion of a phenyl ring around the butadiyne axis. For **BiPtDyTMS**, the lack of the phenyl group eliminates the possibility for differences in conformations caused by the rotation of butadiyne ligands. The simple structure and motion mode of the trimethylsilyl-butadiyne ligand could minimize the rotational/vibrational relaxation in the complex upon excitation, allowing the realization of sharp photoluminescence (fwhm = 10 nm at 298 K and 4 nm at 77 K).

Transient Absorption. To further understand excited state behavior and conformational relaxations that give rise to the excitation wavelength dependent photoluminescence at low temperature, femtosecond transient absorption (fs-TA) experiments were carried out for BiPtDyTMS and BiPtDyP. Figure 4 shows the fs-TA spectra for BiPtDyTMS and BiPtDyP in THF solution over the time scale of 750 fs to 30 ps. BiPtDyTMS (Figure 4a) exhibits two absorption bands in the visible region immediately after the 330 nm excitation pulse. The band around 625 nm decreases in intensity over 15 ps, while the band at 540 nm increases over 15 ps. Global analysis of the kinetics (see Supporting Information, Figure S20a) reveals that the multiwavelength dynamics can be fitted with two time constants with $\tau_1 = 0.26$ ps and $\tau_2 = 2.4$ ps. On the basis of prior work on Pt-acetylide polymers and oligomers, the fast component (τ_1) can be attributed to S_1 to T_1 intersystem crossing (ISC). The slower component (τ_2) is likely due to geometric relaxation in T_1 , possibly involving relaxation of low-frequency modes such as torsion of the carbene ligands around the Pt-C_{carbene} axis. The fs-TA spectra of BiPtDyP are shown in Figure 4b, and it is seen that the spectra feature a single band with a maximum at around 605 nm, the intensity of which increases over the first 30 ps. The global spectral dynamics of this complex were also fitted with two lifetime components with $\tau_1 = 0.31$ ps and $\tau_2 = 4.9$ ps (Supporting Information Figure S20b). Here again, the subpicosecond component is assigned to ISC, while the slower component is assigned to a conformational relaxation related to torsions of the phenylene groups and the carbene ligands. 29,32,42

Qualitatively, the two complexes exhibit similar TA spectral dynamics. Both feature an initial visible transient absorption that undergoes a very rapid change (~300 fs) followed by rapid but comparatively slower process (2-5 ps). As noted above, very similar spectral dynamics have been observed in previous studies of related Pt-acetylide complexes, and they are attributed to $S_1 \rightarrow T_1$ ISC and conformational relaxation.⁴² Interestingly, the TMS-substituted complex, BiPtDyTMS, features two distinct transient absorptions, one at early time (625 nm) that evolves into a stronger band at shorter wavelength (540 nm). By contrast, the phenyl-substituted complex BiPtDyP exhibits only a single transient absorption, the strength of which increases with time following excitation. A possible assignment for the pronounced spectral shift for BiPtDyTMS is that it arises from symmetry breaking and triplet localization onto a single butadiyne moiety. 42 This changes the electronic structure of the T₁ state substantially, which explains the large blue shift of the transient absorption. Due to the greater delocalization in BiPtDyP, triplet localization on a single butadiyne does not give rise to the significant spectral shift.

Organic Light Emitting Diode Application. To explore the application of the two Pt-NHC phosphors in OLEDs, multilayer devices employing BiPtDyP and BiPtDyTMS as emitters were fabricated. OLEDs that utilized BiPtDyP were solution-processed, while the devices utilizing BiPtDyTMS were fabricated via vacuum thermal evaporation. The difference in device processing methods used for the two complexes was due to the observation that BiPtDyP decomposed during heating under high vacuum, whereas BiPtDyTMS was stable under the vacuum thermal evaporation. In order to understand the different thermal behavior of the two complexes, thermogravimetric analysis (TGA) and differential scanning calorimetry (DSC) of BiPtDyP and BiPtDyTMS were carried out in N₂ atmosphere, and the results are shown in Figure S13 in the Supporting Information. Although the conditions are not the same as within the high-vacuum condition inside the thermal evaporation chamber, the result indicates that the decomposition temperature of BiPtDyP is slightly lower than that of BiPtDyTMS. This likely explains why BiPtDyP decomposed while BiPtDyTMS could be deposited by vacuum thermal evaporation. It is also possible that BiPtDyP is less volatile than BiPtDyTMS, and it decomposes before reaching the temperature needed for evaporative deposition. The structures of all the other materials used in OLED fabrication are shown in Figure S14 in the Supporting Information.

For the solution-processed BiPtDyP-based OLEDs, the general device structure was designed by reference to that used for quantum dot-based LEDs. 43-45 As shown schematically in Figure S15, the device was constructed as ITO/PEDOT:PSS (35 nm)/poly-TPD or PVK (35 nm)/DPEPO doped with 15% BiPtDyP (30 nm)/TPBi (30 nm)/LiF (1 nm)/Al (100 nm). Figures S16 and S17 (Supporting Information) show the electroluminescence (EL) spectrum and the corresponding CIE coordinates of BiPtDyP based devices, while the current luminance-voltage characteristics and the external quantum efficiencies are shown in Figures S18 and S19. The electroluminescence of the devices with poly-TPD as the hole transport layer shows a similar band shape as the photoluminescence of BiPtDyP except a moderate contribution of a high energy emission peak at $\lambda_{max} \approx 425$ nm, which can be attributed to the emission of poly-TPD. Changing the hole transport layer to PVK suppressed this feature. As a result, device electroluminescence resembles the photoluminescence of BiPtDyP with CIE coordinates (0.225, 0.427). The maximum EQE increased from 0.4% to 0.8% for the PVK hole transport layer. The relatively poor device performance may be attributed to the nonideal surface morphology of the emissive layer and inadequate energy level alignment of the device, as well as unsatisfactory photoluminescence quantum yield. On the positive side, the blue-green EL spectrum is as narrow as its PL spectrum with a fwhm of 17 nm, so the color purity is maintained.

BiPtDyTMS was used as the emitter in deep-blue emitting OLEDs fabricated by vacuum thermal evaporation. The initial device configuration was ITO/15% MoO₃:85% CzSi (10 nm)/CzSi (5 nm)/DPEPO doped with 15% BiPtDyTMS (20 nm)/TSPO1 (10 nm)/TPBi (30 nm)/LiF (1 nm)/Al (100 nm) (see Figure 5). As shown in Figure 6, the BiPtDyTMS device

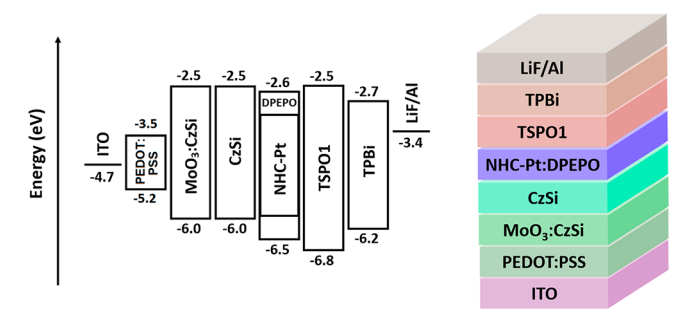


Figure 5. Device structure and energy scheme of BiPtDyTMS based devices.

exhibits deep-blue EL with CIE coordinates (0.172, 0.104) and a maximum EQE of 2.3%. A 35 nm PEDOT:PSS layer was added between the ITO and the MoO₃:CzSi layer. Considering the relatively high energy barrier for hole injection between the anode and MoO₃:CzSi, PEDOT:PSS is used as an extra layer to further overcome the energy barrier (see energy level diagram in Figure 5). As a result, the hole injection efficiency was improved, and this device configuration showed improved performance with a peak EQE of 3.2% and an EL spectrum with a fwhm of 12 nm. Interestingly, the PEDOT:PSS layer also helps to suppress the vibronic sidebands of the emitter (Figure 6a). As a result, the device

displays a slightly deeper blue emission with CIE coordinates of (0.172, 0.086). Compared with solid-state photoluminescence, the suppression of the vibronic sidebands in the OLED electroluminescence further reduces color contamination and results in one of the purest deep-blue colors among the PHOLED research works that have been reported.

Table 3 compares the properties of the state of the art deepblue Ir(III) or Pt(II) based phosphors used in PHOLEDs. Most of the phosphors display either a single broad emission band or a band consisting of several vibronic sub-bands, giving overall emission spectra with fwhm's larger than 20 nm. For BiPtDyTMS, however, the narrow and strong 0–0 band with well-resolved narrow vibronic progressions endows it with an extraordinary pure blue color. Interestingly, while most of the complexes were built based on bidentate ligands (for Ir(III)) or tetradentate ligands (for Pt(II)) to provide a more rigid molecular structure to reduce vibronic transitions, ¹⁶ BiPtDyTMS and BiPtDyP in this work are solely based on monodentate NHC and ancillary butadiyne ligands, and both of them exhibit narrow emission spectra and pure emission color.

Also worthy of note is that the peak wavelength of BiPtDyTMS is as low as 415 nm, which is among the shortest wavelengths, i.e., highest triplet energies of phosphors for PHOLEDs. The high triplet energy helps to push the emission color into deep-blue region but also makes it challenging to identify a stable and efficient host material. As a result, although the device displays superior performance in terms of color purity, the device efficiency needs to be further improved, especially considering the relatively high solid-state quantum yield of BiPtDyTMS. Part of the reason is that the triplet energy of the host material used in this work is not high enough compared with the dopant. As seen in Figure 3a, the 0-0 emission band of BiPtDyTMS at 415 nm indicates a triplet energy of 3.0 eV, while the triplet energy of the DPEPO host material is also \sim 3.0 eV, ⁴⁸ which could possibly allow the host to quench the triplet state of the emitter. This is a common challenge for deep-blue OLEDs, as the triplet energy of the emitter is too high to be matched with an applicable host material. Further device optimization, including host material selection and device engineering, should be able to address this issue.

Despite the relatively low efficiency, another issue of BiPtDyTMS based devices is that they suffer from significant efficiency roll-off. The device with PEDOT:PSS exhibits peak EQE 3.2% at luminance 1 cd/m², while it drops to less than 0.5% at luminance 100 cd/m^2 . One of the reasons could be the unbalanced injection of electrons and holes; especially at higher driving voltage excessive charge carrier accumulation could damage the device. More importantly, the efficiency rolloff could be attributed to triplet-triplet annihilation and triplet-polaron quenching due to the relatively long triplet lifetime of the emitter. As previously discussed, the emission of **BiPtDyTMS** originates from butadiyne ligand centered $^{3}(\pi \rightarrow$ π^*) transitions with a very minor contribution from 3MLCT character. The relatively weak contribution of Pt-based orbitals to the ${}^3(\pi \to \pi^*)$ state leads to weak spin-orbit coupling and consequently a comparatively longer triplet lifetime. By contrast, most of the PHOLEDs in Table 3 do not exhibit sharp efficiency roll-off, especially those that display a broad Gaussian-shaped spectrum, which is a manifestation of ³MLCT dominated emission 49 and therefore stronger spin-orbit coupling and relatively shorter lifetimes. While the device

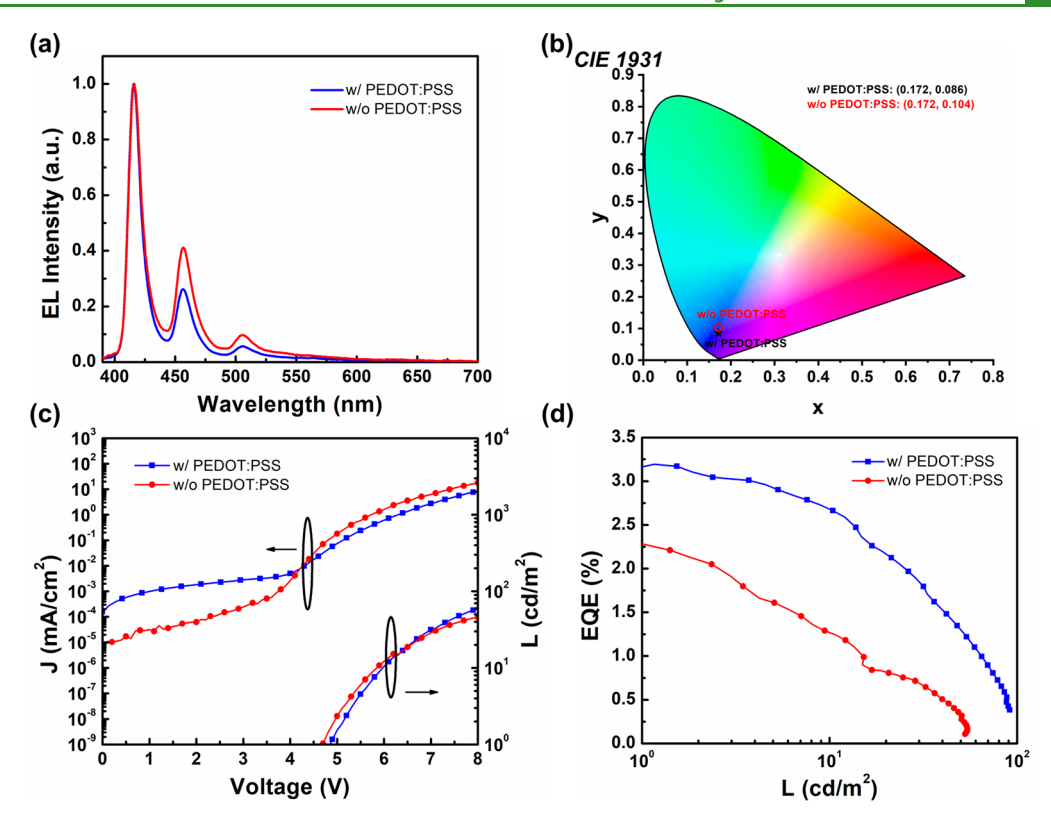


Figure 6. (a) Electroluminescence spectra, (b) CIE coordinates, (c) J-V-L characterics (J = current density, L = luminance), and (d) external quantum efficiency (EQE) versus luminance L for **BiPtDyTMS** based devices.

efficiency roll-off issue needs to be resolved, the color purity of the EL device in this work illustrates how a pure deep-blue emission can be achieved through molecular structural design, combined with smart device engineering.

CONCLUSIONS

We report the synthesis, characterization, and OLED application of two novel trans-NHC platinum(II) complexes featuring butadiyne functionalities. These two complexes exhibit sharp photoluminescence with fwhm of <15 nm in both solution and solid-state PMMA matrix at room temperature. The blue-green emitter BiPtDyP displays a solid-state quantum yield of 32% in PMMA (2 wt %). More importantly, BiPtDyTMS achieves a saturated deep-blue emission with CIE coordinates of (0.163, 0.077), a 0-0 band fwhm of 10 nm, and a relatively high quantum yield of 57% in PMMA. PHOLEDs employing these two emitters display electroluminescence that closely matches the corresponding photoluminescence. It is noteworthy that the BiPtDyTMS based devices maintain the sharp emission shape with a fwhm of 12 nm and show deep-blue CIE coordinates of (0.172, 0.086), which approaches the NTSC coordinates for "pure" blue. Although further device engineering is needed to improve the brightness and efficiency of the OLED, this work suggests that butadiyne ligands not only give rise to new structures for Pt(II)-based phosphorescent emitters but also extend the scope of PHOLEDs development.

■ EXPERIMENTAL SECTION

Synthesis. Synthesis, characterization, and X-ray structural data are included in the Supporting Information.

Photophysical Properties. UV-vis absorption spectra were recorded on a Shimadzu UV-2600 spectrophotometer. Steady-state

emissions in THF and solid-state were measured on an Edinburgh FLS-1000 photoluminescence spectrometer. The solutions were degassed with N2 for 30 min before measurement. The quantum yields of complexes doped into poly(methyl methacrylate) (PMMA) thin films were obtained using a SM4 integrating sphere mounted on Edinburgh FLS-1000 photoluminescence spectrometer. The quantum yields of complexes in THF were obtained with a Photon Technology International (PTI) fluorometer and determined relative to a standard of 9,10-diphenyl anthracene in cyclohexane, which has a reported fluorescence quantum yield of 0.90.50 The solution samples for quantum yields were deoxygenated through four cycles of freezepump-thaw technique before measurements. Phosphorescence lifetime measurements were carried out using an Edinburgh LP920 spectrophotometer (Edinburgh Instruments) and a tunable OPOTEK Radiant 355 LD series ($\lambda = 355$ nm) as the excitation source. Femtosecond transient absorption data were obtained by using a pump-probe technique with a 120 fs, 1 kHz Ti:sapphire (Coherent Astrella) laser. The pump beam was generated using a portion of the 800 nm amplifier beam by being directed into an optical parametric amplifier (OPerA Solo, Coherent), which was tuned to generate a beam of light of 330 nm. The 330 nm pump beam was then directed into a Helios Fire (Ultrafast Systems) automated femtosecond transient absorption spectrometer where the beam passed through a mechanical chopper and neutral density filter to tune the beam to 100 μW of power before hitting the stirred sample (~0.2 OD). Meanwhile, another portion of the 800 nm beam was directed into the Helios Fire directed into an automated 8 ns delay stage; afterward, the beam was focused on a sapphire plate to generate a visible probe ranging from 430 to 750 nm. The signal was detected using a fibercoupled alignment-free spectrometer with a 1024 pixel CMOS sensor. The data were analyzed by the Surface Xplorer data analysis software.

PMMA Films Fabrication. PMMA (98 mg or 85 mg, 35 kDa) was added to dichloromethane (DCM) (1.0 mL) and stirred at room temperature for 24 h. The respective platinum complex (2 mg, 2 wt % or 15 mg, 15 wt %) was added to the solution and stirred for another 1 h. The resulting solution was drop casted onto a glass substrate and dried at room temperature for 2 days inside an Erlab Captair Flow

Table 3. Comparison of PHOLEDs Based on Different Deep-Blue Phosphors

Phosphor	Ф _{PL} ^a	λ _{EL} (nm) ^b	FWHM -	EC	RE (%)	CIE (x,y)	Ref
				Max	@ 100 cd/m ²		
F ₅ C NN CF ₃	0.47	430	63	13.4	12.5	(0.15, 0.05)	46
	0.66	418	~ 66	10.1	9.0 ^d	(0.16, 0.09)	25
	0.54	431	~70 ^e	22.5	16.5	(0.15, 0.11)	17
	0.91	451	29	24.8	22.7	(0.15, 0.08)	18
	0.83	451	~20	15.4	12.3	(0.15, 0.17)	47
Bu-N-y-N-Bu Bu-N-y-Bu	0.56	439	35	14.1	10.2	(0.16, 0.13)	41
This work	0.57	415	12	3.2	0.5	(0.17, 0.09)	

^aPhotoluminescence quantum yield measured in solid-state. ^bElectroluminescence maximum. ^cfwhm is estimated from the dominant emission peak in EL. ^dMeasured at 1000 cd/m². ^eConvoluted dominating peaks in the spectrum.

391 fume hood in the dark. Pure PMMA films were made as the reference via the same method. Complex/DPEPO thin films were fabricated following the same procedure.

OLED Fabrication and Device Testing. OLED fabrication was performed according to the methods reported previously.^{51,52} The devices were fabricated on glass substrates commercially precoated with a layer of indium tin oxide (ITO) with a sheet resistance of ~15 Ω /sq. The substrates were cleaned with soapy water, deionized water, acetone, and isopropanol, consecutively, and then exposed to ultraviolet ozone for 15 min immediately before device construction. For solution-processed BiPtDyP devices, the treated substrates were spin-coated with poly(ethylenedioxythiophene):polystyrene sulfonate (PEDOT:PSS) (AI 4083) and annealed at 150 °C for 15 min in air. The coated substrates were then transferred into a nitrogen-filled glovebox for further spin-coating. Poly(N,N'-bis-4-butylphenyl-N,N'bisphenyl)benzidine (poly-TPD) or poly(9-vinylcarbazole) (PVK) was dissolved in chlorobenzene and then spin-coated onto the substrates followed by annealing at 150 °C for 30 min. BiPtDyP and bis[2-(diphenylphosphino)phenyl]ether oxide (DPEPO) were dissolved in chlorobenzene with a 15%:85% weight ratio and then spincoated onto the substrates followed by annealing at 150 °C for 30 min. The substrates were then loaded into a high-vacuum deposition chamber (background pressure lower than 4×10^{-6} Torr), and 2,2',2"-(1,3,5-benzinetriyl)-tris(1-phenyl-1*H*-benzimidazole) (TPBi), LiF, and aluminum cathode were deposited in succession without breaking the vacuum. For vacuum-deposited BiPtDyTMS devices, the

treated substrates (with or without PEDOT:PSS layer) were directly loaded into a high-vacuum deposition chamber (background pressure lower than 4 \times 10^{-6} Torr). MoO_3 and 9-(4-tert-butylphenyl)-3,6-bis(triphenylsilyl)-9H-carbazole (CzSi) with 15%:85% volume ratio, pristine CzSi, BiPtDyTMS and DPEPO with 15%:85% volume ratio, diphenyl[4-(triphenylsilyl)phenyl]phosphine oxide (TSPO1), TPBi, LiF, and aluminum cathode were deposited in succession without breaking the vacuum. For all the devices fabricated, a crossbar geometry was used for the patterned ITO anode and the Al cathode, which defined an active device area of 4 mm².

The electroluminescence spectra of the OLEDs were obtained using an Ocean Optics spectrometer (USB 2000) and a Keithley 2400 power source. Current-density-voltage (J-V) characteristics of the devices were measured using an Agilent 4155C semiconductor parameter analyzer under ambient conditions. The luminance was calculated from the photocurrent of a calibrated silicon detector (Newport 818 UV) that was placed close to the devices assuming Lambertian emission. The external quantum efficiencies were then calculated from luminance and device spectra.

ASSOCIATED CONTENT

Supporting Information

The Supporting Information is available free of charge at https://pubs.acs.org/doi/10.1021/acsami.0c21193.

Experimental details, NMR spectra, X-ray crystallography summary table, photoluminescence lifetime data, and OLED data (PDF)

Crystallographic information, BiPtDyTMS (CIF) Crystallographic information, BiPtDyP (CIF)

AUTHOR INFORMATION

Corresponding Author

Kirk S. Schanze — Department of Chemistry, University of Texas at San Antonio, San Antonio, Texas 78249, United States; orcid.org/0000-0003-3342-4080; Email: kirk.schanze@utsa.edu

Authors

- Ru He Department of Chemistry, University of Florida, Gainesville, Florida 32611, United States; Department of Chemistry, University of Texas at San Antonio, San Antonio, Texas 78249, United States
- Zhengtao Xu Department of Materials Science and Engineering, University of Florida, Gainesville, Florida 32611, United States
- Silvano Valandro Department of Chemistry, University of Texas at San Antonio, San Antonio, Texas 78249, United States; Ocid.org/0000-0002-4652-768X
- Hadi D. Arman Department of Chemistry, University of Texas at San Antonio, San Antonio, Texas 78249, United States
- Jiangeng Xue Department of Materials Science and Engineering, University of Florida, Gainesville, Florida 32611, United States

Complete contact information is available at: https://pubs.acs.org/10.1021/acsami.0c21193

Notes

The authors declare no competing financial interest.

■ ACKNOWLEDGMENTS

This work was supported by the National Science Foundation (Grant CHE-1904288) to K.S.S. J.X. and Z.X. acknowledge support from the National Science Foundation (Grants DMR-1609306, CHE-1904534) and NSF Grant MRI 1920057.

REFERENCES

- (1) Tang, C. W.; VanSlyke, S. A. Organic Electroluminescent Diodes. Appl. Phys. Lett. 1987, 51 (12), 913–915.
- (2) Im, Y.; Byun, S. Y.; Kim, J. H.; Lee, D. R.; Oh, C. S.; Yook, K. S.; Lee, J. Y. Recent Progress in High-Efficiency Blue-Light-Emitting Materials for Organic Light-Emitting Diodes. *Adv. Funct. Mater.* **2017**, 27 (13), 1603007.
- (3) Kelley, T. W.; Baude, P. F.; Gerlach, C.; Ender, D. E.; Muyres, D.; Haase, M. A.; Vogel, D. E.; Theiss, S. D. Recent Progress in Organic Electronics: Materials, Devices, and Processes. *Chem. Mater.* **2004**, *16* (23), 4413–4422.
- (4) Uoyama, H.; Goushi, K.; Shizu, K.; Nomura, H.; Adachi, C. Highly Efficient Organic Light-Emitting Diodes from Delayed Fluorescence. *Nature* **2012**, 492 (7428), 234–238.
- (5) Pfeiffer, M.; Leo, K.; Zhou, X.; Huang, J.; Hofmann, M.; Werner, A.; Blochwitz-Nimoth, J. Doped Organic Semiconductors: Physics and Application in Light Emitting Diodes. *Org. Electron.* **2003**, *4* (2-3), 89–103.
- (6) Farinola, G. M.; Ragni, R. Electroluminescent Materials for White Organic Light Emitting Diodes. *Chem. Soc. Rev.* **2011**, *40* (7), 3467–3482.

- (7) Baldo, M. A.; O'Brien, D. F.; You, Y.; Shoustikov, A.; Sibley, S.; Thompson, M. E.; Forrest, S. R. Highly Efficient Phosphorescent Emission from Organic Electroluminescent Devices. *Nature* **1998**, 395 (6698), 151–154.
- (8) Tung, Y. L.; Lee, S. W.; Chi, Y.; Chen, L. S.; Shu, C. F.; Wu, F. I.; Carty, A. J.; Chou, P. T.; Peng, S. M.; Lee, G. H. Organic Light-Emitting Diodes Based on Charge-Neutral Ru^{II} Phosphorescent Emitters. *Adv. Mater.* **2005**, *17* (8), 1059–1064.
- (9) Baldo, M.; Lamansky, S.; Burrows, P.; Thompson, M.; Forrest, S. Very High-Efficiency Green Organic Light-Emitting Devices Based on Electrophosphorescence. *Appl. Phys. Lett.* **1999**, *75* (1), 4–6.
- (10) Li, G.; Zhu, D.; Peng, T.; Liu, Y.; Wang, Y.; Bryce, M. R. Very High Efficiency Orange-Red Light-Emitting Devices with Low Roll-Off at High Luminance Based on an Ideal Host-Guest System Consisting of Two Novel Phosphorescent Iridium Complexes with Bipolar Transport. Adv. Funct. Mater. 2014, 24 (47), 7420-7426.
- (11) Su, Y. J.; Huang, H. L.; Li, C. L.; Chien, C. H.; Tao, Y. T.; Chou, P. T.; Datta, S.; Liu, R. S. Highly Efficient Red Electrophosphorescent Devices Based on Iridium Isoquinoline Complexes: Remarkable External Quantum Efficiency over a Wide Range of Current. Adv. Mater. 2003, 15 (11), 884–888.
- (12) Zhu, Y. C.; Zhou, L.; Li, H. Y.; Xu, Q. L.; Teng, M. Y.; Zheng, Y. X.; Zuo, J. L.; Zhang, H. J.; You, X. Z. Highly Efficient Green and Blue-Green Phosphorescent OLEDs Based on Iridium Complexes with the Tetraphenylimidodiphosphinate Ligand. *Adv. Mater.* **2011**, 23 (35), 4041–4046.
- (13) Lo, S. C.; Male, N. A.; Markham, J. P.; Magennis, S. W.; Burn, P. L.; Salata, O. V.; Samuel, I. D. Green Phosphorescent Dendrimer for Light-Emitting Diodes. *Adv. Mater.* **2002**, *14* (13–14), 975–979.
- (14) Kondo, Y.; Yoshiura, K.; Kitera, S.; Nishi, H.; Oda, S.; Gotoh, H.; Sasada, Y.; Yanai, M.; Hatakeyama, T. Narrowband Deep-Blue Organic Light-Emitting Diode Featuring an Organoboron-Based Emitter. *Nat. Photonics* **2019**, *13* (10), 678–682.
- (15) Takada, N.; Tsutsui, T.; Saito, S. Control of Emission Characteristics in Organic Thin-Film Electroluminescent Diodes Using an Optical-Microcavity Structure. *Appl. Phys. Lett.* **1993**, *63* (15), 2032–2034.
- (16) Li, G.; Fleetham, T.; Turner, E.; Hang, X. C.; Li, J. Highly Efficient and Stable Narrow-Band Phosphorescent Emitters for OLED Applications. *Adv. Opt. Mater.* **2015**, *3* (3), 390–397.
- (17) Li, X.; Zhang, J.; Zhao, Z.; Wang, L.; Yang, H.; Chang, Q.; Jiang, N.; Liu, Z.; Bian, Z.; Liu, W.; Lu, Z.; Huang, C. Deep Blue Phosphorescent Organic Light-Emitting Diodes with CIEy Value of 0.11 and External Quantum Efficiency up to 22.5%. *Adv. Mater.* **2018**, 30 (12), 1705005.
- (18) Fleetham, T.; Li, G.; Wen, L.; Li, J. Efficient "Pure" Blue OLEDs Employing Tetradentate Pt Complexes with a Narrow Spectral Bandwidth. *Adv. Mater.* **2014**, 26 (41), 7116–7121.
- (19) Weaver, M.; Tung, Y. J.; D'Andrade, B.; Esler, J.; Brown, J.; Mackenzie, P.; Walters, R.; Tsai, J. Y.; Brown, C.; Lin, C. 11.1: Invited Paper: Advances in Blue Phosphorescent Organic Light-Emitting Devices. SID Symposium Digest of Technical Papers; Wiley Online Library, 2006; pp 127–130.
- (20) Tamayo, A. B.; Alleyne, B. D.; Djurovich, P. I.; Lamansky, S.; Tsyba, I.; Ho, N. N.; Bau, R.; Thompson, M. E. Synthesis and Characterization of Facial and Meridional Tris-Cyclometalated Iridium (III) Complexes. J. Am. Chem. Soc. 2003, 125 (24), 7377–7387.
- (21) Yang, C. H.; Cheng, Y. M.; Chi, Y.; Hsu, C. J.; Fang, F. C.; Wong, K. T.; Chou, P. T.; Chang, C. H.; Tsai, M. H.; Wu, C. C. Blue-Emitting Heteroleptic Iridium (III) Complexes Suitable for High-Efficiency Phosphorescent OLEDs. *Angew. Chem., Int. Ed.* **2007**, 46 (14), 2418–2421.
- (22) Na, H.; Teets, T. S. Highly Luminescent Cyclometalated Iridium Complexes Generated by Nucleophilic Addition to Coordinated Isocyanides. *J. Am. Chem. Soc.* **2018**, *140* (20), 6353–6360.

- (23) Lowry, M. S.; Hudson, W. R.; Pascal, R. A.; Bernhard, S. Accelerated Luminophore Discovery through Combinatorial Synthesis. *J. Am. Chem. Soc.* **2004**, *126* (43), 14129–14135.
- (24) You, Y.; Park, S. Y. Inter-Ligand Energy Transfer and Related Emission Change in the Cyclometalated Heteroleptic Iridium Complex: Facile and Efficient Color Tuning over the Whole Visible Range by the Ancillary Ligand Structure. *J. Am. Chem. Soc.* **2005**, *127* (36), 12438–12439.
- (25) Lee, J.; Chen, H.-F.; Batagoda, T.; Coburn, C.; Djurovich, P. I.; Thompson, M. E.; Forrest, S. R. Deep Blue Phosphorescent Organic Light-Emitting Diodes with Very High Brightness and Efficiency. *Nat. Mater.* **2016**, *15* (1), 92–98.
- (26) Na, H.; Canada, L. M.; Wen, Z.; Wu, J. I-C.; Teets, T. S. Mixed-Carbene Cyclometalated Iridium Complexes with Saturated Blue Luminescence. *Chem. Sci.* **2019**, *10* (25), 6254–6260.
- (27) Fleetham, T.; Li, G.; Li, J. Phosphorescent Pt (II) and Pd (II) Complexes for Efficient, High-Color-Quality, and Stable OLEDs. *Adv. Mater.* **2017**, 29 (5), 1601861.
- (28) Zhou, G.; Wong, W. Y.; Yang, X. New Design Tactics in OLEDs Using Functionalized 2-Phenylpyridine-Type Cyclometalates of Iridium (III) and Platinum (II). *Chem. Asian J.* **2011**, *6* (7), 1706–1727.
- (29) Bullock, J. D.; Salehi, A.; Zeman, C. J., IV; Abboud, K. A.; So, F.; Schanze, K. S. In Search of Deeper Blues: Trans-N-Heterocyclic Carbene Platinum Phenylacetylide as a Dopant for Phosphorescent OLEDs. ACS Appl. Mater. Interfaces 2017, 9 (47), 41111–41114.
- (30) Li, Y.; Winkel, R. W.; Weisbach, N.; Gladysz, J. A.; Schanze, K. S. Photophysics of Platinum Tetrayne Oligomers: Delocalization of Triplet Exciton. *J. Phys. Chem. A* **2014**, *118* (45), 10333–10339.
- (31) Haque, A.; Al-Balushi, R. A.; Al-Busaidi, I. J.; Khan, M. S.; Raithby, P. R. Rise of Conjugated Poly-ynes and Poly (metalla-ynes): From Design through Synthesis to Structure—Property Relationships and Applications. *Chem. Rev.* **2018**, *118* (18), 8474—8597.
- (32) Bullock, J. D.; Valandro, S. R.; Sulicz, A. N.; Zeman, C. J., IV; Abboud, K. A.; Schanze, K. S. Blue Phosphorescent Trans-N-Heterocyclic Carbene Platinum Acetylides: Dependence on Energy Gap and Conformation. *J. Phys. Chem. A* **2019**, *123* (42), 9069–9078.
- (33) Che, C.-M.; Chao, H.-Y.; Miskowski, V. M.; Li, Y.; Cheung, K.-K. Luminescent μ -Ethynediyl and μ -Butadiynediyl Binuclear Gold(I) Complexes: Observation of $^3(\pi\pi^*)$ Emissions from Bridging C_n²⁻Units. *J. Am. Chem. Soc.* **2001**, *123* (21), 4985–4991.
- (34) Zhang, Y.; Blacque, O.; Venkatesan, K. Highly Efficient Deep-Blue Emitters Based on *cis* and *trans* N-Heterocyclic Carbene Pt^{II} Acetylide Complexes: Synthesis, Photophysical Properties, and Mechanistic Studies. *Chem. Eur. J.* **2013**, *19* (46), 15689–15701.
- (35) Szafert, S.; Gladysz, J. Update 1 Of: Carbon in One Dimension: Structural Analysis of the Higher Conjugated Polyynes. *Chem. Rev.* **2006**, *106* (11), PR1–PR33.
- (36) de Quadras, L.; Shelton, A. H.; Kuhn, H.; Hampel, F.; Schanze, K. S.; Gladysz, J. A. Syntheses, Structures, and Electronic and Photophysical Properties of Unsymmetrically Substituted Butadiyne-diyl and Hexatriynediyl Complexes Derived from $(C_6F_5)(R_3P)_2Pt$, $(p-tol)(R_3P)_2Pt$, and $(Ph_3P)Au$ End-Groups. Organometallics **2008**, 27 (19), 4979–4991.
- (37) Zheng, Q.; Bohling, J. C.; Peters, T. B.; Frisch, A. C.; Hampel, F.; Gladysz, J. A Synthetic Breakthrough into an Unanticipated Stability Regime: A Series of Isolable Complexes in Which C_6 , C_8 , C_{10} , C_{12} , C_{16} , C_{20} , C_{24} , and C_{28} Polyynediyl Chains Span Two Platinum Atoms. *Chem. Eur. J.* **2006**, *12* (25), 6486–6505.
- (38) Nagano, Y.; Ikoma, T.; Akiyama, K.; Tero-Kubota, S. Symmetry Switching of the Fluorescent Excited State in α,ω -Diphenylpolyynes. *J. Am. Chem. Soc.* **2003**, *125* (46), 14103–14112.
- (39) Zhuravlev, F.; Gladysz, J. A. Electronic Structure and Chain-Length Effects in Diplatinum Polyynediyl Complexes trans,trans- $[(X)(R_3P)_2Pt(C\equiv C)_nPt(PR_3)_2(X)]$: A Computational Investigation. *Chem. Eur. J.* **2004**, 10 (24), 6510–6522.
- (40) Glusac, K.; Köse, M. E.; Jiang, H.; Schanze, K. S. Triplet Excited State in Platinum— Acetylide Oligomers: Triplet Localization

- and Effects of Conformation. J. Phys. Chem. B 2007, 111 (5), 929-940.
- (41) Bullock, J. D.; Xu, Z.; Valandro, S.; Younus, M.; Xue, J.; Schanze, K. S. Trans-N-(Heterocyclic Carbene) Platinum (II) Acetylide Chromophores as Phosphors for OLED Applications. *ACS Appl. Electron. Mater.* **2020**, 2 (4), 1026–1034.
- (42) Ramakrishna, G.; Goodson, T., III; Rogers-Haley, J. E.; Cooper, T. M.; McLean, D. G.; Urbas, A. Ultrafast Intersystem Crossing: Excited State Dynamics of Platinum Acetylide Complexes. *J. Phys. Chem. C* 2009, 113 (3), 1060–1066.
- (43) Sun, Q.; Wang, Y. A.; Li, L. S.; Wang, D.; Zhu, T.; Xu, J.; Yang, C.; Li, Y. Bright, Multicoloured Light-Emitting Diodes Based on Quantum Dots. *Nat. Photonics* **2007**, *1* (12), 717–722.
- (44) Qian, L.; Zheng, Y.; Xue, J.; Holloway, P. H. Stable and Efficient Quantum-Dot Light-Emitting Diodes Based on Solution-Processed Multilayer Structures. *Nat. Photonics* **2011**, *5* (9), 543–548.
- (45) Chen, H.; Ding, K.; Fan, L.; Liu, W.; Zhang, R.; Xiang, S.; Zhang, Q.; Wang, L. All-Solution-Processed Quantum Dot Light Emitting Diodes Based on Double Hole Transport Layers by Hot Spin-Coating with Highly Efficient and Low Turn-on Voltage. ACS Appl. Mater. Interfaces 2018, 10 (34), 29076–29082.
- (46) Pal, A. K.; Krotkus, S.; Fontani, M.; Mackenzie, C. F.; Cordes, D. B.; Slawin, A. M.; Samuel, I. D.; Zysman-Colman, E. High-Efficiency Deep-Blue-Emitting Organic Light-Emitting Diodes Based on Iridium (III) Carbene Complexes. *Adv. Mater.* **2018**, *30* (50), 1804231.
- (47) Wang, X.; Peng, T.; Nguyen, C.; Lu, Z. H.; Wang, N.; Wu, W.; Li, Q.; Wang, S. Highly Efficient Deep-Blue Electrophosphorescent Pt (II) Compounds with Non-Distorted Flat Geometry: Tetradentate versus Macrocyclic Chelate Ligands. *Adv. Funct. Mater.* **2017**, 27 (4), 1604318.
- (48) Zhang, Q.; Komino, T.; Huang, S.; Matsunami, S.; Goushi, K.; Adachi, C. Triplet Exciton Confinement in Green Organic Light-Emitting Diodes Containing Luminescent Charge-Transfer Cu (I) Complexes. *Adv. Funct. Mater.* **2012**, 22 (11), 2327–2336.
- (49) Lamansky, S.; Djurovich, P.; Murphy, D.; Abdel-Razzaq, F.; Lee, H.-E.; Adachi, C.; Burrows, P. E.; Forrest, S. R.; Thompson, M. E. Highly Phosphorescent Bis-Cyclometalated Iridium Complexes: Synthesis, Photophysical Characterization, and Use in Organic Light Emitting Diodes. J. Am. Chem. Soc. 2001, 123 (18), 4304–4312.
- (50) Hamai, S.; Hirayama, F. Actinometric Determination of Absolute Fluorescence Quantum Yields. *J. Phys. Chem.* **1983**, 87 (1), 83–89.
- (51) Zheng, Y.; Eom, S.-H.; Chopra, N.; Lee, J.; So, F.; Xue, J. Efficient Deep-Blue Phosphorescent Organic Light-Emitting Device with Improved Electron and Exciton Confinement. *Appl. Phys. Lett.* **2008**, 92 (22), 223301.
- (52) Yang, Y.; Cohn, P.; Eom, S.-H.; Abboud, K. A.; Castellano, R. K.; Xue, J. Ultraviolet-Violet Electroluminescence from Highly Fluorescent Purines. *J. Mater. Chem. C* **2013**, *1* (16), 2867–2874.